Ground-state hyperfine measurement in laser-trapped radioactive ^{21}Na

M. A. Rowe, S. J. Freedman, B. K. Fujikawa, G. Gwinner, S.-Q. Shang, and P. A. Vetter
Department of Physics, University of California at Berkeley and Lawrence Berkeley National Laboratory, Berkeley, California 94720
(Received 15 September 1998)

We have measured the ground-state hyperfine splitting between the $3S_{1/2}$ $F=2, m=0$ and $3S_{1/2}$ $F=1, m=0$ levels of ^{21}Na. The measurement was performed with microwave spectroscopy on 40 000 radioactive ^{21}Na atoms ($t_{1/2}=22$ sec) collected in a magneto-optical trap on-line at the 88-in cyclotron at LBNL. The transition was excited with microwaves directed at the atoms and detected with resonant probe fluorescence light. The splitting ν_{HFS} in a zero magnetic field was determined to be 1 906 471 870$\pm$200 Hz.
[S1050-2947(99)02503-2]

PACS number(s): 32.30.−r

I. INTRODUCTION

We have made a precise determination of the hyperfine splitting of the $3S_{1/2}$ ground state of ^{21}Na. This measurement, the first microwave transition observed in laser trapped radioactive atoms, took advantage of the long observation time and sensitive detection available with atoms nearly at rest in a trap to make a measurement on relatively few atoms. This technique can be useful in rare and short-lived alkalis for precise hyperfine spectroscopy on strings of isotopes [1]. We are exploring microwave spectroscopy on ^{21}Na primarily as a means of characterizing to $<1\%$ uncertainty the nuclear polarization of an optically pumped group of atoms. In work with a cesium atomic beam [2] magnetic sublevel populations have been determined to less than one percent by probing individual sublevels with microwaves. A simple replacement of the microwave by a pair of laser beams configured to make Raman transitions allows a purely optical determination of polarization with the same technique [3]. Precise knowledge of nuclear polarization will allow the physics of interest to be extracted from β decay measurements. For instance, the experimentally observed up/down asymmetry of the β's emitted from polarized nuclei requires a measure of polarization to extract the β-asymmetry coefficient. This coefficient is sensitive to deviations from the fundamental V-A (vector−axial-vector) structure of the charged current weak interaction in the Standard Model [4].

Radioactive isotopes confined in neutral atom traps will play an important role in future precision measurements of weak interactions such as the parity violating asymmetry in the β decay of spin-polarized nuclei, electron-neutrino correlation, and parity violation in atoms [5]. Radioactive atom trapping can provide a solution to the difficult task of improving current β decay measurements because it provides a localized, isotopically pure sample in which source scattering is eliminated. In this situation both the β particle and the recoiling daughter ion from the β decay are available for study with their momenta unperturbed. Neutral atoms are easily manipulated by optical pumping techniques to achieve the high nuclear spin polarization necessary for precise spin-polarized correlation measurements. Loading a trap with atoms, turning off the trap, turning on an alignment field, optically polarizing the atoms, measuring the decay and repeating will provide a clean, well described environment in which to study the decay. With these goals in mind we have performed microwave spectroscopy on trapped ^{21}Na atoms.

II. TRAPPING APPARATUS

Here we give a brief summary of our trapping apparatus along with recent changes. For more details see our previous paper on trapping ^{21}Na [6]. Figure 1 shows the layout of our trapping setup. The experiment starts with the production of ^{21}Na in a heated target. The magnesium target in [6] has been replaced with magnesium oxide. This highly refractory material remains solid while the produced sodium diffuses from the target. This is advantageous because there is essentially no depletion of the target material and the vapor pressure is low in the target. The target consists of a stack of 8, 40 mg, 1-cm-diam pressed disks of magnesium oxide powder with a maximum grain size of 40 μm. The disks are

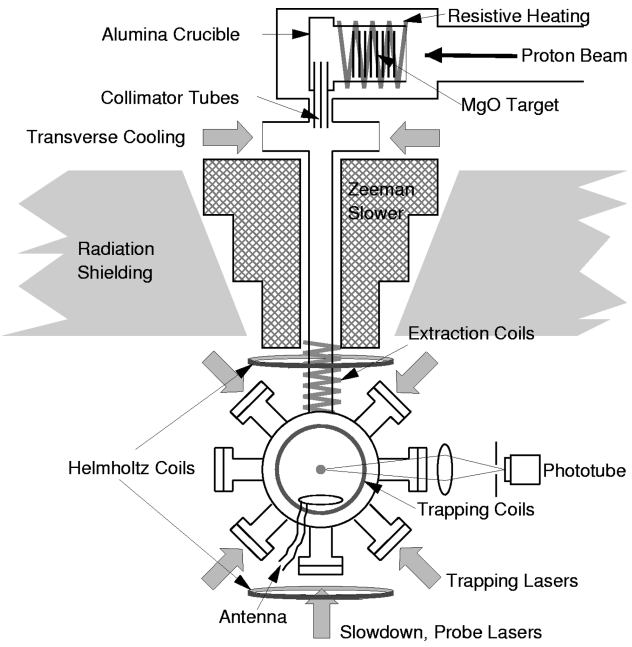

FIG. 1. Layout of the trapping apparatus that shows relative placement and is not drawn to scale.

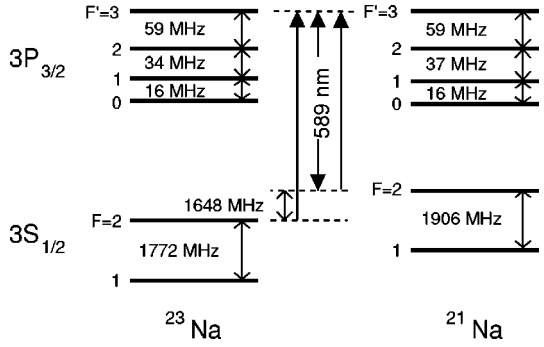

FIG. 2. D_2 lines of ^{23}Na and ^{21}Na. The natural linewidth of this transition is 10 MHz.

spaced equally apart in a tantalum holder and placed in a 2.5-cm-long alumina crucible. A tiny grain of sodium oxide (≈ 0.5 mg) is added to the crucible to supply a ^{23}Na beam for tests and calibration. The crucible is heated to about 1000 °C in an oven which uses a spiral cut tantalum piece for resistive heating. ^{21}Na is produced with 1 μA of 25-MeV protons provided by the 88-in cyclotron at Lawrence Berkeley National Laboratory. The nuclear reaction ^{24}Mg(p,α)^{21}Na is used to produce the 22-sec half-life isotope. An atomic beam is extracted from the target through four small holes in the crucible. Both passive and active collimation are used to direct the ^{21}Na atomic beam as it leaves the target's crucible holes. We have installed four, 1.3-cm-long, 0.65-mm-inner-diam Ta tubes in the exit holes from the crucible. The refractory target results in a low gas viscosity environment inside the atomic beam oven, resulting in an enhanced forward flux from the Ta channels by a factor of 15 [7]. Active collimation consists of a transverse cooling stage where a red detuned laser beam is passed multiple times across the atomic beam in both transverse dimensions. A 1 cm diameter beam with a total power of 100 mW produces a tenfold increase in forward flux.

The cooling and trapping laser beams are generated by a Coherent model 899 ring dye laser run at 589 nm using Rhodamine 6G dye. It is externally locked by saturation absorption spectroscopy to a transition of the D_2 line of natural sodium, ^{23}Na, shown in Fig. 2. The isotope shift between ^{23}Na and ^{21}Na, 1648 MHz, is compensated by a high-frequency acousto-optic modulator (AOM). This AOM shifts the frequency of the beam entering the saturation absorption locking loop up by 1648 MHz, resulting in the beams sent to the experiment being lowered by 1648 MHz relative to the ^{23}Na case. An electro-optic modulator (EOM) gives the laser sideband frequencies, providing a second frequency ($F=1$ to $F'=2$) in addition to the trapping one ($F=2$ to $F'=3$) to prevent optical pumping to the $F=1$ level. The power in this sideband is 15% of the total. To change from trapping ^{23}Na to ^{21}Na the EOM input frequency is simply changed to account for the different ground-state splittings of the two isotopes and the beam sent into the saturated absorption locking loop is frequency shifted up by the isotope shift. A 1.2-m-long Zeeman slower [8] embedded in the concrete shielding wall between the target and trap regions is used in combination with a slowdown laser to cool the atoms in the atomic beam for loading into the magneto-optic trap. The slowdown beam propagates through the magneto-optic trap, into the Zeeman slower and focuses on the oven exit aperature. The slowdown is detuned by approximately three natural linewidths to the red of the $F=2$ to $F=3$ transition to minimize trap disruption. The slowdown beam is circularly polarized with 8 mW/cm^2 in a 2-cm diameter. A uniform transition is made from the magnetic field at the end of the Zeeman slower to the trapping field by a set of extraction coils, allowing the atoms to be smoothly loaded into the trap. The trapping field is a quadrupole field with a gradient of ≈ 20 G/cm along the axial direction. In addition, an arbitrary constant bias field can be applied along the atomic beam direction with two sets of Helmholtz coils. One pair of Helmholtz coils is switchable and the other is always on. The vacuum pressure in the trapping chamber is $\approx 5\times 10^{-10}$ torr. We use 80 mW of laser power in a 2-cm-diam beam to make the six trapping laser beams. The power is divided into two beams. One is recycled among the four horizontal beams and the other makes the upward beam and a retroreflected downward beam. The mean intensity of each trapping beam is 20 mW/cm^2. The trapping beams are red detuned about 13 MHz from the $F=2$ to $F'=3$ transition. Currently this set-up gives us 40 000 ^{21}Na atoms in our trap with which to perform measurements.

TABLE I. Data cycle.

Time (ms)	Event
−15	fields lowered
−3	trap size measured
0	shut off EOM
0.2	trap beams off
0.3	magnetic fields off
0.4	slowdown laser off
3.8–4.8	microwave pulse
4.8–5.05	probe atoms

III. HYPERFINE MEASUREMENT TECHNIQUE

The hyperfine measurement consists of exciting the trapped atoms from the $3S_{1/2}$ $F=1$, $m=0$ level to the $3S_{1/2}$ $F=2$, $m=0$ level with a microwave pulse and detecting transitions via fluorescence on the $F=2$ to $F'=3$ transition in a technique described in [9]. Each microwave frequency measurement involves a cycle of optical manipulations. Cycles at different frequencies are combined to make a complete sweep of the frequency range desired to map the Rabi resonance. Each data set consists of many sweeps averaged together. The experiment is run with National Instruments data acquisition boards, a counter board NB-TIO-10, a general I/O board NB-MIO-16XL, a GPIB board NB-GPIB/TNT and Labview software. These control the experiment's timing, GPIB communication with the HP 8660C synthesizer, analog inputs and outputs, and photon counting as well as data acquisition and storage. Table I shows the timeline of the data cycle. The cycle starts with about 40 000 trapped atoms. Before the main cycle, the extraction coils are turned off in approximately 10 ms. At the same time the trapping quadrupole field is reduced to half of its normal value and the bias field is adjusted to maintain the trap's position. Then a phototube in current integration mode

measures the optical fluorescence from the trap for trap size normalization. The main cycle begins by turning off the EOM. This removes the repumping frequency and optically pumps atoms to $F=1$. The six main trapping beams are then shut off. Then the quadrupole field and a fraction of the bias field (controlled by the current balance between the switching and nonswitching Helmholtz coil pairs) is rapidly turned off. Changing the switched field fraction allows the measurement to be performed at different magnetic field amplitudes. The fields are rapidly switched by using shaped voltage pulses input to bipolar operational amplifier power supplies (Kepco BOP 50-2M, 36-12M). Next the slowdown laser is shut off.

Eddy currents in our stainless steel vacuum chamber require waiting approximately 4 ms after shutting off the magnetic fields before applying the microwave pulse. This delay was determined by measuring the field shift of ν_{HFS} as a function of the delay time. After approximately 4 ms, the measured ν_{HFS} no longer depended on delay time, indicating that the eddy current fields had decayed. After this delay the atoms receive a 1-ms microwave pulse. The microwave power is adjusted by fitting the resonance line shape so it is about a π pulse. The microwave antenna is a single loop about 3 cm in diameter with 7-cm leads connected to a vacuum feedthrough. The antenna is located around the slowdown beam, approximately 3 cm from the trapped atoms. Power is supplied to the antenna by a Hewlett Packard 8660C synthesized signal generator, amplified with a Hewlett Packard 8349B microwave amplifier.

After the microwave pulse, the atoms are probed to determine how many have been driven from $F=1$ to $F'=2$. The probe laser, aimed along the slowdown direction, is on for 0.25 ms. The probe laser intensity is 600 $\mu\mathrm{W/cm}^2$. It is tuned to resonance for $F=2$ to $F'=3$. This cycling transition results in tens of photons produced for each atom now in $F=2$. The photons are detected by a phototube and the individual pulses are discriminated and counted. The microwave frequency, trap size, and photon counts for the cycle are digitized and stored. Then the trap is turned back on and the atoms are recaptured. More atoms are loaded into the trap for 0.5 sec and a new cycle is begun.

A complete sweep of the desired microwave frequencies takes about 100 sec. Initial inputs for scan width and number of steps define a set of discrete frequencies for the data taking program to investigate. When performing the experiment with a simple, linear scan of microwave frequencies we obtained asymmetric line shapes for the hyperfine resonance. By looking at the trap size data we verified that the effect was caused by trap population loss during our measurement cycle. When the microwave frequency is resonant, atoms transferred to the $F=2$ state by the microwave pulse are ejected by the probe beam from the recapture region of the MOT. This produces a diminished signal size on subsequent microwave frequencies. We addressed this problem by using a microwave interrogation of frequencies at random. This averages trap size fluctuations across the entire line shape. Differences in trap population at each microwave frequency are directly corrected for by normalizing the fluorescence pulse by the trap size brightness measurement taken before each point.

A data set is made up of many sweeps, usually five to ten, taken at a fixed bias field. We also took five cycles of background data at the end of each data set. This allowed us to identify the photon count background and the trap size background caused by laser light reflected off the vacuum chamber. Data sets were taken with six different magnetic bias fields. For each different magnetic bias field, data was taken for both ^{21}Na and ^{23}Na. The ^{23}Na data allowed us to calibrate the bias field strength by comparing to the known zero field splitting of ^{23}Na.

IV. EXPERIMENTAL RESULTS

The raw data was sorted by frequency and trap size. At the time of the experiment, our laser was suffering from brief losses of frequency lock for about 10 ms due to air bubbles in the dye jet. These frequency excursions were usually to the blue of $F=2\rightarrow3$ and ejected the atoms from the trap. Therefore it was necessary to cut these episodes from the data. Only photon count data that have a trap size greater than a certain fixed cutoff are retained and binned by frequency. After applying these cuts that require a minimum trap size, approximately 50% variation in trap size remained for a data set. A statistical error for photon counts is created by taking the square root of the number of accepted photon counts. The photon counts and trap size backgrounds were identified from the final five data cycles of each set. Finally a signal $S(f)$ for each frequency in a data set was produced where

$$S(f)=\frac{C(f)-C_{\mathrm{back}}}{T(f)-T_{\mathrm{back}}} \tag{1}$$

and $C(f)$ is the photon counts, C_{back} is the photon counts background, $T(f)$ is the trap size, and T_{back} is the trap size background. For each of the 25 data sets $S(f)$ was fitted with a Rabi resonance shape that was broadened an amount parametrized by a frequency spread:

$$R(f)=B+A\sum_{i=\pm}\frac{\Gamma^2}{\left[2\pi\left(f-f_0\pm\frac{\Delta f}{2}\right)\right]^2+\Gamma^2}\times\sin^2\left(\sqrt{\left[2\pi\left(f-f_0\pm\frac{\Delta f}{2}\right)\right]^2+\Gamma^2}\,\frac{t}{2}\right) \tag{2}$$

Here A is the amplitude, B is the offset, f_0 is the center frequency, Δf is the frequency spread, f is the varying frequency, Γ is the microwave power parameter, and $t=1$ ms is the fixed microwave pulse time. During the measurement the atoms are released from the trap and expand ballistically outward. The atom cloud samples the magnetic field over a volume a few millimeters in radius. The resonant frequency shifts quadratically with the applied magnetic bias field so magnetic field inhomogeneities over the region the atoms occupy during the microwave pulse cause a spread of the resonant frequency. For our data these are typically a few hundred Hz. Other shifts, such as the Doppler shift (~10 Hz), are small in comparison. The frequency spread parameter in the fit Δf, accounts for this spread. As Δf increases the fit $R(f)$ becomes double peaked (the two individual Rabi shapes become resolved) and it no longer ac-

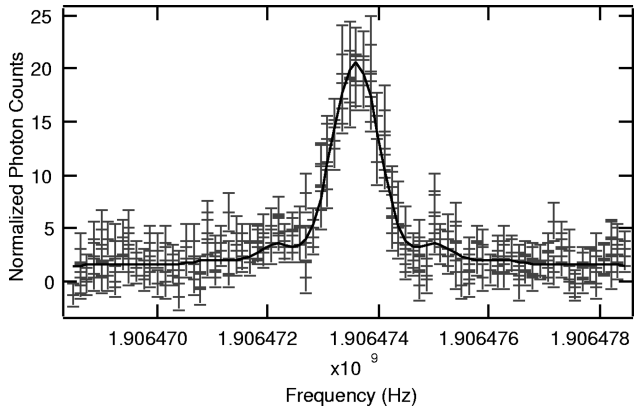

FIG. 3. Plot of ^{21}Na hyperfine resonance data taken in a 0.91-G field.

counts for the additional broadening. In this case a Lorentzian is an appropriate fitting function as it represents a blurred Rabi shape with the side oscillations averaged out. Data at two bias field settings, 0.6 and 2.1 G had extra broadening and were fit with Lorentzians. The errors assigned to this data reflected the additional peak smearing. The final fits give a listing of peak values and statistical errors for each data set. Figure 3 shows an example of a fitted hyperfine resonance for ^{21}Na.

Additional data sets were taken off line with ^{23}Na to estimate systematic errors by purposely varying experimental parameters. Data was taken over the range of about 10 000–200 000 trapped atoms. These errors were grouped into two catagories, local and global. The local errors are caused by run to run variations in experimental parameters. Table II gives a list indicating the typical variation of a parameter and the error it would contribute. For instance, the overall laser power to the trap can change by up to 10 mW during a run causing a 20-Hz shift. Combining the local errors gives a total local error of 60 Hz. The global errors are due to differential frequency shifts between ^{21}Na and ^{23}Na. Shifts resulting from frequency pulling by a resonant vacuum chamber cavity are estimated to be less than 10 Hz based on microwave power absorption measurements with a network analyzer. The dominant error here is caused by our uncertainty in the equality of absolute trap laser detunings between ^{23}Na and ^{21}Na. Possible inaccuracies in the absolute EOM frequencies for the two isotopes added to the global error.

The local systematic error was added in quadrature with the statistical error of the peak for each of the 25 data sets. Next the peak values taken at the same magnetic bias field were combined and the peak frequency was obtained for each of the six bias field values. From the Breit-Rabi formula [10] for an $m=0$ to $m=0$ transition:

$$\Delta\nu_{\mathrm{HFS}}=\frac{(g_J\mu_B)^2}{2h^2\nu_{\mathrm{HFS}}}B^2 \tag{3}$$

$$=2.228B^2 \ \ \mathrm{kHz/G^2\ for\ ^{23}Na}, \tag{4}$$

$$=2.071B^2 \ \ \mathrm{kHz/G^2\ for\ ^{21}Na}, \tag{5}$$

resulting in

$$B(\mathrm{G})=\sqrt{0.4488\times[\Delta\nu_{\mathrm{HFS}}(^{23}\mathrm{Na})\ (\mathrm{kHz})]}, \tag{6}$$

$$\Delta\nu_{\mathrm{HFS}}(^{21}\mathrm{Na})=0.9295\Delta\nu_{\mathrm{HFS}}(^{23}\mathrm{Na}), \tag{7}$$

where B is the bias field strength. The shift from the known zero field value for ^{23}Na$=1\,771\,626\,129$ Hz [11] was calculated for each bias field value and the bias magnetic field strength was determined via Eq. (6). Figure 4 shows the peak values for ^{21}Na as a function of the bias magnetic field strength. The corresponding frequency shifts ranged from 0.5 kHz to almost 9 kHz. The data are fit with

$$F(B)=F_0+2071 \ \ B^2\mathrm{Hz/G^2} \tag{8}$$

to determine F_0, the zero-field splitting value. This is equivalent to subtracting the shift, $2071B^2$, and taking the weighted average of the remainders (see the residual plot). The error in the zero field splitting value for ^{21}Na results from the original error in the ^{21}Na peak plus the error in the extrapolation back to zero field, which is 93% of the error in the ^{23}Na peak [see Eq. (7)]. The fit resulted in a value of the zero field splitting for ^{21}Na equal to $1\,906\,471{,}870\pm30$ Hz with $\chi^2=7$ $(n=6)$. Our largest error was global. There can be an overall offset between ^{21}Na and ^{23}Na of 160 Hz. This error is dominated by the overall laser frequency detuning,

TABLE II. Systematic errors.

Local systematic errors	Maximum experimental variation	Error used
Probe frequency	1 MHz	7 Hz
Slowdown frequency	1 MHz	2 Hz
Repump power/main mode power	15 ± 5 %	50 Hz
Probe power	100 μW	10 Hz
Trapping beams power	10 mW	20 Hz
Slowdown power	1 mW	20 Hz
Global systematic errors		
Cooling laser detuning	5 MHz	140 Hz
EOM frequency	5 MHz	70 Hz
Synthesizer calibration	constant offset	10 Hz
Resonant cavity frequency pulling		10 Hz

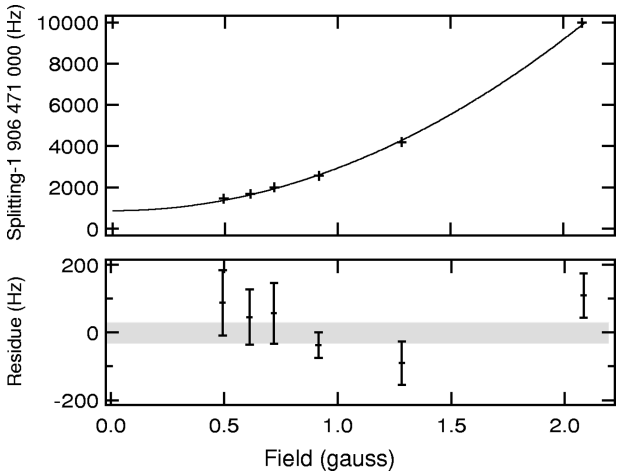

FIG. 4. Plot of the peak values of the ^{21}Na hyperfine resonances as a function of the bias magnetic field strength.

which can be made better with simple improvements to the laser lock and electronically controlled switching between isotopes. Adding all errors in quadrature, our result is $\nu_{\mathrm{HFS}}(^{21}\mathrm{Na}) = 1\,906\,471\,870 \pm 200$ Hz.

V. CONCLUSION

This experiment strongly demonstrates how trapping techniques can be applied to spectroscopy of unstable isotopes. The trap measurement of the ground-state hyperfine splitting of ^{21}Na improves by a factor of 100 the previous measurement performed with an atomic beam [12]. Another factor of ten improvement could be made with closer attention to systematics but with the same basic apparatus. With a complimentary measurement of the magnetic moment of ^{21}Na to 10^{-5} (via hyperfine structure in a large magnetic field) it is possible to measure the Bohr-Weisskopf effect [1] for ^{21}Na to learn about the spatial distribution of the nuclear polarization. This result also indicates that microwave spectroscopy is a promising technique for precise polarization data, neccessary for polarized β decay experiments, with small amounts of rare short-lived radioactive atoms. In addition to the $m=0$ to $m=0$ transition the $m=\pm 1$ to $m=0$ transitions can be excited. Here the transitions shift linearly with the applied magnetic field, 700 Hz/mG, so field inhomogeneities cause more peak smearing. Better field uniformity and/or higher microwave power to broaden the peaks can make these transitions measurable. Then by comparing peak heights the relative populations in the three magnetic sublevels can be determined in order to determine a net polarization after optical pumping in a polarized nucleus β decay experiment.

ACKNOWLEDGMENTS

This work was supported by the Office of Energy Research, Office of Basic Energy Sciences, of the U.S. Department of Energy under Contract No. DE-AC03-76SF00098.

[1] H.T. Duong *et al.*, CERN-PPE/92-147.
[2] B.P. Masterson, C. Tanner, H. Patrick, and C.E. Wieman, Phys. Rev. A **47**, 2139 (1993).
[3] C.S. Wood *et al.*, Science **275**, 1759 (1997).
[4] O. Naviliat-Cuncic, T.A. Girard, J. Deutsch, and N. Severijns, J. Phys. G **17**, 919 (1991).
[5] G.D. Sprouse and L.A. Orozco, Annu. Rev. Nucl. Part. Sci. **47**, 429 (1997).
[6] Z-T. Lu *et al.*, Phys. Rev. Lett. **72**, 3791 (1994).
[7] V. Hughes and H. Schultz, *Methods of Experimental Physics* (Academic Press, New York, 1967), Vol. 4, p. 162.
[8] W.D. Phillips and H. Metcalf, Phys. Rev. Lett. **48**, 596 (1982); V.S. Bagnato, *et al.*, J. Opt. Soc. Am. B **6**, 2171 (1989).
[9] D.W. Sesko and C.E. Wieman, Opt. Lett. **14**, 269 (1989).
[10] A. Corney, *Atomic and Laser Spectroscopy* (Oxford University Press, Oxford, 1988).
[11] A. Beckmann, K. Böklen, and D. Elke, Z. Phys. **270**, 173 (1974).
[12] O. Ames, E. Phillips, and S. Glickstein, Phys. Rev. **137**, B1157 (1965).